Astron. Astrophys. 290, 819–833 (1994)

ASTRONOMY AND ASTROPHYSICS

Towards an understanding of very massive stars. A new evolutionary scenario relating O stars, LBVs and Wolf-Rayet stars

N. Langer[1], W.-R. Hamann[2,3], M. Lennon[2], F. Najarro[2], A.W.A. Pauldrach[2], and J. Puls[2]

[1] Max-Planck-Institut für Astrophysik, Karl-Schwarzschild-Str. 1, Postfach 1523, D-85740 Garching b. München, Germany
[2] Universitäts-Sternwarte München, Scheinerstr. 1, D-81679 München, Germany
[3] Institut für Theoretische Physik und Sternwarte der Universität, Olshausenstraße, D-24118 Kiel, Germany

Received 9 March 1994 / Accepted 21 May 1994

Abstract. Based on recent progress in the theory of stellar structure and evolution, in the theory of stellar atmospheres and winds, and in the observational data base, we propose a new scenario for the evolution of very massive stars ($M_{\rm ZAMS} \gtrsim 40 M_\odot$) in our Galaxy. A sample evolutionary calculation for a $60 M_\odot$ star, incorporating recent theoretical results about violent pulsational instabilities in very massive stars, is critically compared with a multitude of observational facts. The relation between those pulsational instabilities and observed line profile variability in O stars is discussed. New wind models for P Cygni are computed, with particular emphasis on the determination of its mass and surface He/H-ratio. A detailed comparison of our sequence with the Galactic WR population is performed, considering newly determined surface abundances.

Our results suggest a new interpretation of luminous hydrogen-rich late-type WN stars as core hydrogen burning objects, while hot WN stars with small or zero hydrogen abundance are core helium burning stars. P Cygni is identified with the hydrogen shell burning phase of our sequence. The observed upper luminosity limit for Galactic hydrogen-free WN stars appears to be consistent with our picture. Hence we propose the following evolutionary sequence for very massive stars: O → Of → H-rich WN → LBV → H-poor WN → H-free WN → WC → SN.

Key words: stars: abundances – stars: evolution – stars: mass-loss – stars: Wolf-Rayet – stars: supergiants

1. Introduction

In the recent past, great progress has been made in observations of very massive stars (VMS) and their quantitative interpretation. The atmospheric parameters and helium abundances of several very luminous O and Of stars have been determined by means of non-LTE, although still hydrostatic, model atmospheres (e.g. Simon et al. 1983; Voels et al. 1989; Herrero et al. 1992 – for a review see Kudritzki & Hummer 1990). For the same kind of stars, stellar wind parameters were obtained from UV (e.g., Howarth & Prinja 1989; Groenewegen & Lamers 1989), Hα (Leitherer 1988) or radio observations (Bieging et al. 1989). Wolf-Rayet (WR) stars — the potential descendants of O stars (cf. Lamers et al. 1991) — have been analyzed equally successful, with the consequence that luminosities, mass-loss rates and surface compositions of a large fraction of them are now known (Hamann et al. 1993; Koesterke 1993). For Luminous Blue Variables (LBVs), a considerable amount of information has been accumulated (cf. Sect. 4), the best studied example being P Cygni (see Davidson et al. 1989).

Also for the stellar models, considerable progress has been achieved recently. A major improvement in the radiative opacities (Iglesias et al. 1992; Seaton et al. 1994), which has already been shown to remove several longstanding discrepancies with observations for stars less massive than those considered here (see e.g. Iglesias et al. 1992), leads to large changes for evolutionary tracks of very massive stars (see e.g. Schaller et al. 1992; Stothers & Chin 1991). Furthermore, a large fraction of possible VMS models has been found to be violently pulsationally unstable on the core hydrogen burning main sequence (Kiriakidis et al. 1993) and on the helium main sequence (Glatzel et al. 1993).

However, instead of clarifying our knowledge of VMS evolution, most of the recent discoveries have revealed new discrepancies between VMS models and observational results: O stars appear to be often more luminous and more He-enriched than corresponding models (Herrero et al. 1992), and some of them (e.g. extreme Of stars) show mass-loss rates which may exceed those predicted by the theory of radiation-driven winds (Lamers & Leitherer 1993). VMS main sequence models (cf. Schaller et al. 1992; Stothers & Chin 1981) evolve beyond the Humphreys-Davidson (HD) limit in the HR diagram where no normal stars are observed (Humphreys & Davidson 1979; Blaha & Humphreys 1989). The observed upper luminosity limit for

Send offprint requests to: N. Langer

Galactic hydrogen-free WN stars (Hamann et al. 1993, cf. also Sect. 5) is largely violated by VMS post main sequence models (cf. e.g. Schaller et al. 1992; Bressan et al. 1993). Observational data of P Cygni (Pauldrach & Puls 1990; de Groot & Lamers 1992), e.g. its very low mass, cannot be reproduced by standard stellar models (El Eid & Hartmann 1993). Observed LBV outbursts and WR-type mass outflows are not theoretically understood, while violent pulsational instabilities are predicted theoretically but not observed.

In view of all these problems one may conclude that VMS evolution is still far from being established. Consequently, the standard scenario for VMS evolution along the spectral sequence O → LBV → WR, which corresponds to the internal evolutionary path of core-H burning → shell-H burning → core-He burning (Maeder 1983; Langer & El Eid 1986; Maeder & Meynet 1987), must be regarded as provisional.

In the present paper, we attempt to include the results of the pulsational analysis of Kiriakidis et al. (1993) in stellar evolution calculations, though only in a qualitative and parametric way (cf. Sect. 2). However, as we show below, it enables us to suggest an evolutionary scenario for VMS which is quite different from the standard one. A critical comparison of the resulting stellar models with observations, considering the fundamental problems mentioned above, is performed for O stars in Sect. 3, for LBVs, especially P Cygni, in Sect. 4, and for WR stars in Sect. 5. In Sect. 6 we discuss remaining problems with our model and propose further possible tests. The conclusions are summarized in Sect. 7.

2. Stellar evolution calculations

2.1. Input physics and assumptions

We have calculated the evolution of a $60 M_\odot$ star with metallicity $Z = 0.02$ from the Zero Age Main Sequence (ZAMS) through core He-exhaustion with an implicit Lagrangian hydrodynamic code (cf. Langer 1991b) with up-to-date input physics. In particular, the latest version of the OPAL opacities (Iglesias et al. 1992) is used. For convection we adopt the model of Langer et al. (1983), with no extra mixing, neither convective overshooting nor rotationally induced mixing (cf. Langer 1992). However, note that especially the assumptions on convection are not critical to the present investigation, since the evolution of VMS is primarily mass-loss dominated (cf. Langer 1993).

For the mass-loss we adopt the rate proposed by Lamers & Leitherer (1993) during the O star phase. However, — and this is the essential assumption in this study — for models which have been shown to be violently pulsationally unstable by Kiriakidis et al. (1993), we use an enhanced mass-loss rate: Kiriakidis et al. have studied a $60 M_\odot$ star with $Z = 0.02$ (which corresponds to our example) and found it to be unstable to radial pulsations in the $T_{\rm eff}$-range 42 000 K $\gtrsim T_{\rm eff} \gtrsim$ 22 000 K, with remarkably short growth times of the instability of the order of only a few times the dynamical time scale at $T_{\rm eff} \simeq 30\,000$ K. We make the simplistic but plausible assumption, that this extremely violent instability drives a mass outflow at a rate inversely proportional to the instability growth time. More specifically, we adopt a mass-loss rate of

$$\dot{M} = 3.358\,10^{-4}\, f\,(4.63 - \log T_{\rm eff}/{\rm K}) M_\odot\ {\rm yr}^{-1} \quad \text{for} \quad 4.63 > \log T_{\rm eff}/{\rm K} > 4.535 \qquad (1)$$

$$\dot{M} = 1.636\,10^{-4}\, f\,(\log T_{\rm eff}/{\rm K} - 4.34) M_\odot\ {\rm yr}^{-1} \quad \text{for} \quad 4.535 > \log T_{\rm eff}/{\rm K} > 4.34 \qquad (2)$$

which makes use of a linear fit to $\sigma_{\rm i}$, the imaginary part of the eigenfrequency obtained by Kiriakidis et al. (cf. their Fig. 7b). The proportionality factor f is chosen as $f = 1$ for our main calculations, which yields about $3\,10^{-5} M_\odot\ {\rm yr}^{-1}$ at $\log T_{\rm eff}/{\rm K} = 4.535$ as maximum mass-loss rate. This is the order of magnitude expected from preliminary non-linear hydrodynamical calculations of the instabilities (Kiriakidis 1992). The same order of magnitude of the mass-loss emerges from the estimate that the layer above the iron opacity bump (which is supposed to drive the pulsations) is ejected after about 10 pulsation periods. Note that the assumption of Wolf-Rayet type mass-loss rates due to violent pulsations is supported by the results of Glatzel et al. (1993), who find the same kind of instability as discussed above for models of helium stars in a wide mass range (cf. Sect. 6).

In our calculations we also take into account, for the first time, the effect of a partly optically thick outflowing envelope by specifying appropriate outer boundary conditions (cf. Höflich & Langer, in prep., for details). Consequently, the backwarming effect of the optically thick parts of the wind ("wind-blanketing") is self-consistently included in the structure of our models. The final aim of this procedure is to compute meaningful stellar "surface" temperatures and radii for models with large mass-loss rates; however, since the accelerating forces in the transition region from optically thick to optically thin parts of the wind cannot yet be theoretically predicted, we have to adopt a wind velocity law for our outer boundary condition, i.e.

$$v(r) = v_{\rm N} + (v_\infty - v_{\rm N}) \left(1 - \frac{R_*}{r}\right)^\beta , \qquad (3)$$

where $v_{\rm N}$ is the velocity at our outermost grid point, and v_∞ is the final wind velocity. v_∞ and β are parameters, which are adopted as $\beta = 1$ and v_∞ as function of $v_{\rm esc}$ in accordance with observations. In order to determine the optical thickness of the layers above our outermost grid point, also the opacity coefficient in these layers has to be specified (which we adopt to $\kappa_{\rm wind} = 0.2\,{\rm cm}^2\ {\rm g}^{-1}$). With these assumptions we compute an effective temperature at $\tau_{\rm Ross} = 2/3$ which we designate as $T_{\rm eff}$. Note that as long as the three a priori unknown parameters (β, v_∞, and $\kappa_{\rm wind}$) cannot be computed theoretically, the obtained surface temperatures for the case of strong mass loss (i.e. $\tau_{\rm wind} \gtrsim 1$) cannot be expected to be quantitatively reliable.

2.2. Core hydrogen burning

The core-H burning phase of our $60 M_\odot$ model sequence computed with $f = 1$ evolves as in standard calculations (cf. e.g.

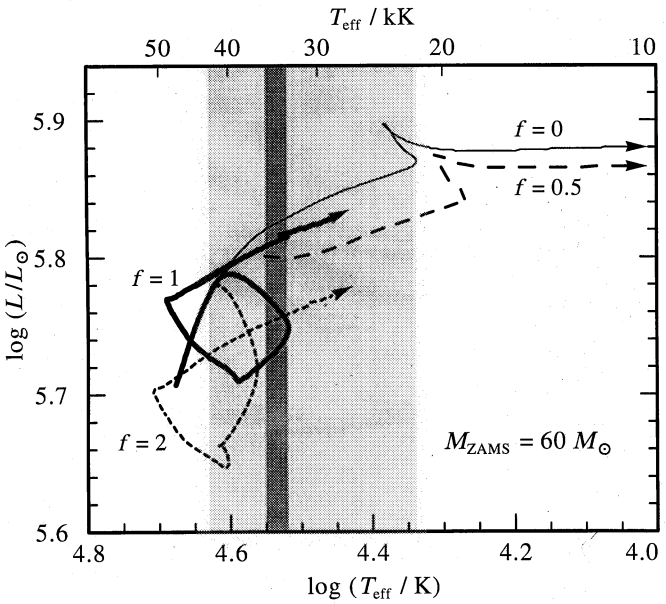

Fig. 1. Evolutionary tracks during core hydrogen burning and early shell hydrogen burning for stars of initially $60M_\odot$, with different choices of the parameter f (labels) which scales the additional mass-loss due to violent pulsations (cf. Eqs. 1 and 2). The region where pulsationally enhanced mass-loss is assumed is shown shaded, with the maximum rate occurring at the dark shaded effective temperature

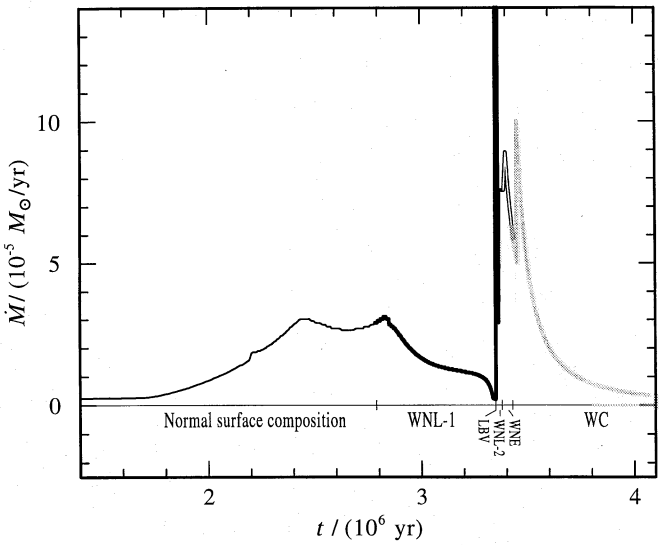

Fig. 2. Mass-loss rate (in $M_\odot\,{\rm yr}^{-1}$) versus time (in 10^6 yr) for our $60M_\odot$ sequence ($f = 1.0$). The spectral types according to surface abundances are indicated, and distinguished by different drawing styles. The peak of $\dot{M}$ during the LBV phase reaches $5\,10^{-3}M_\odot\,{\rm yr}^{-1}$, removing an amount of $6M_\odot$ during this short-lived stage

Schaller et al. 1992) for the first $\sim 2\,10^6$ yr (up to a central helium mass fraction of $Y_{\rm c} \simeq 0.6$, i.e. 60% of the core hydrogen burning life time), which is the time when the stellar surface temperature decreases below $\sim 40\,000$ K (cf. Table 1 and Fig. 1) and the pulsationally driven mass-loss becomes dominant. Up to this time, the stellar mass has decreased from 60 to about $56M_\odot$. Figure 1 shows also evolutionary tracks for which the factor f in Eqs. (1) and (2) is set to 0.5 and 2, respectively, compared with our standard example ($f = 1$) and with a track without the additional, pulsationally driven mass-loss ($f = 0$).

Figure 2 shows the time variation of the mass-loss rate for our main track ($f = 1$). At $Y_{\rm c} \simeq 0.75$, the maximum mass-loss rate of $3\,10^{-5}M_\odot\,{\rm yr}^{-1}$ is reached (cf. Sect. 2.1), and thereafter the mass-loss decreases towards core H-exhaustion, a behavior which reflects the evolutionary path in the HR diagram. From Fig. 1 it is obvious that for $f \gtrsim 0.5$ (i.e. $\dot{M}_{\rm max} \gtrsim 1.5\,10^{-5}M_\odot\,{\rm yr}^{-1}$) the mass-loss is strong enough in order to keep the star to the blue side of the instability region in the HR diagram, i.e. the star avoids surface temperatures cooler than $\sim 30\,000$ K during its main sequence phase.

Due to the enhanced mass-loss, the star with $f = 1$ terminates core-H burning with a total mass of $26.4M_\odot$. Its surface hydrogen mass fraction has decreased to $X_{\rm s} = 0.28$, corresponding to a surface number ratio of $n_{\rm He}/n_{\rm H} \simeq 0.54$. Due to the decreasing mass, the convective core has decreased much more rapidly than in standard calculations, and has a mass of only $16.2\,M_\odot$ at core H-exhaustion (cf. also Fig. 4a, below). Note that this fixes the initial mass of the helium core.

2.3. Shell hydrogen burning

Now we discuss the further evolution along our main track ($f = 1$). The position of core hydrogen exhaustion in the HR diagram is approximately at $\log T_{\rm eff}/{\rm K} = 4.6$ and $\log L/L_\odot = 5.7$. This is much hotter and less luminous compared to standard calculations, and lies within the main sequence band. As in standard evolution calculations, the core H-exhaustion is followed by an overall contraction phase, which is terminated when the ignition of the H-burning shell forces the stellar radius to increase, while the He-core continues to contract (cf. Fig. 1). In the course of this envelope expansion, our sequence crosses the pulsational instability regime in the HR diagram, but due to the short time spent there it is without consequences for the further evolution of the star.

However, when the stellar surface temperature continues to decrease, the star is expected to become more and more violently unstable. E.g. for surface temperatures below $\sim 20\,000$ K, Kiriakidis et al. (1993) predict instabilities triggered by the He- and H-recombination zones which are stronger than the iron-bump instability which occurred during the main sequence evolution. Moreover, all these instabilities are known to increase with increasing L/M-ratio, which implies that the instabilities in our $60M_\odot$ sequence should become increasingly stronger than the ones predicted by Kiriakidis et al., who applied only standard mass-loss to their $60M_\odot$ sequence. It should be noted also that Stothers & Chin (1993, 1994) predict the occurrence of a dynamical instability for extended and luminous post-main sequence stars, which might apply as well to our sequence during the hydrogen shell burning phase. However, though Stothers & Chin claim to have found this instability in linear and non-linear cal-

Table 1. Various quantities as function of time, describing our main $60M_\odot$ track ($f = 1$). Y_c and Y_s denote central and surface helium mass fraction, O_c is the central oxygen mass fraction, T_c and ρ_c are central temperature and density, and the other symbols have their usual meanings.

t	M	$\log \dot{M}$	$\log L$	$T_{\rm eff}$	Y_c	Y_s	O_c	$M_{\rm conv}$	T_c	ρ_c
10^6 yr	$M_\odot$	$M_\odot\,{\rm yr}^{-1}$	$L_\odot$	kK				$M_\odot$	10^8 K	g cm^{-3}
0.020	59.9	5.77	5.71	47.6	.28	.28	.01	42.2	0.41	2.23
1.342	57.4	5.63	5.77	43.1	.50	.28	.00	34.0	0.41	2.09
2.042	54.5	5.00	5.80	38.9	.64	.28	.00	29.3	0.42	2.26
2.608	42.4	4.57	5.76	31.6	.78	.31	.00	23.9	0.43	2.80
3.085	30.7	4.87	5.73	38.9	.90	.60	.00	19.4	0.46	3.74
3.348	27.9	5.48	5.74	42.6	.98	.68	.00	17.0	0.59	8.01
3.363	20.7	4.12	5.86	30.0	.95	.88	.00	10.6	1.98	$3.80\,10^2$
3.384	19.1	4.12	5.65	82.6	.88	.90	.00	12.3	1.99	$3.85\,10^2$
3.395	18.1	4.03	5.61	77.3	.84	.98	.00	12.2	1.99	$4.00\,10^2$
3.433	15.3	4.22	5.48	85.3	.73	.98	.01	11.4	1.99	$4.50\,10^2$
3.520	10.0	4.40	5.19	82.3	.55	.68	.04	6.7	1.98	$6.19\,10^2$
4.006	4.1	5.40	4.53	111.1	.01	.31	.62	2.1	2.49	$2.63\,10^3$
4.065	3.9	5.46	5.01	95.5	.00	.28	.00	0.0	25.3	$1.62\,10^7$

culations, its existence could not be confirmed by Glatzel (priv. communication).

In any case it appears reasonable to assume that, during its redward evolution after shell hydrogen ignition, the stellar envelope becomes sufficiently destabilized in order to loose mass at a rate in excess of that used for the main sequence instability. In our calculations, we apply a mass-loss rate of $5\,10^{-3} M_\odot\,{\rm yr}^{-1}$ in that phase, until the direction of the evolution in the HR diagram is reversed and the temperature at the stellar surface exceeds again 20 000 K. Let us note that the value of $5\,10^{-3} M_\odot\,{\rm yr}^{-1}$ is not a well determined quantity, and its exact choice may affect to some extent the amount of mass of the remaining H-rich envelope and thereby the surface He/H-ratio at the time when the star returns to the hot side of the HR diagram.

2.4. Core helium burning

When the star returns from its short excursion to the cool side of the HR diagram, central helium burning has just established, and the helium core has achieved thermal equilibrium thereby. A hydrogen containing envelope of $2.5M_\odot$ has remained on the star (note again that its exact amount may depend somewhat on the mass-loss rate applied in the H-shell burning phase; cf. Sect. 2.3), which is sufficient to maintain a hydrogen burning shell source which first contributes considerably ($\sim 40\%$) to the total luminosity. The surface hydrogen mass fraction of our sequence at the beginning of core He-burning is $X_s \simeq 0.1$ (i.e. $n_{\rm He}/n_{\rm H} \simeq 2$).

By identifying our core helium burning models with Wolf-Rayet stars (cf. Sect. 5), we apply appropriate empirical and semi-empirical mass-loss rates in our calculations. As long as hydrogen is present at the stellar surface, we adopt a constant mass-loss rate of $7.5\,10^{-5} M_\odot\,{\rm yr}^{-1}$ according to observed mass-loss rates of the most luminous WN stars (Hamann et al. 1993). This leads to the removal of the remaining hydrogen within a time of $\sim 3\,10^4$ yr. Due to the corresponding decrease in the luminosity generated by the H-burning shell, the stellar luminosity at the time when the surface hydrogen abundance vanishes is $\log L/L_\odot = 5.61$ (cf. also Fig. 9). This is considerably less than the corresponding value from the $60M_\odot$ sequence of Schaller et al. (1992), i.e. $\log L/L_\odot = 5.98$.

After the hydrogen abundance has decreased to zero, we continued the computations with the mass dependent mass-loss rate of Langer (1989b). The carbon enriched WC phase is reached at $M_* = 15.3M_\odot$, $Y_c = 0.73$, and $\log L/L_\odot = 5.48$, starting with a brief phase of simultaneous nitrogen and carbon enrichment lasting $\sim 2\,10^4$ yr (cf. Langer 1991a). The final mass of the star is $3.92M_\odot$, which makes it a probable candidate for a supernova explosion (Woosley et al. 1993).

Note that the complete evolution of the star in the HR diagram is shown below in Fig. 8.

3. Pulsational instability and observed O star variability

The HRD in Fig. 3 shows the results of the linear pulsational stability analysis for massive stars with solar metallicity ($Z = 0.02$) as obtained by Kiriakidis et al. (1993). Unstable phases are shaded. Dark shading refers to very unstable phases, defined somewhat arbitrarily by the criterion that the growth time of the pulsations is less than 20 times the dynamical time scale. Superimposed are the observed positions of stars investigated for optical line profile variations (*lpv*). The size of the symbols is proportional to the relative amplitude of variability observed in He I λ5876. These data are from the spectroscopic survey of Galactic O stars conducted by Fullerton et al. (in prep.; see also Fullerton 1990, 1991). It consists of a magnitude-limited sample of 30 stars, and is therefore biased toward intrinsically more luminous objects.

The coincidence between the region of observed non-variability and variability and the theoretical onset of insta-

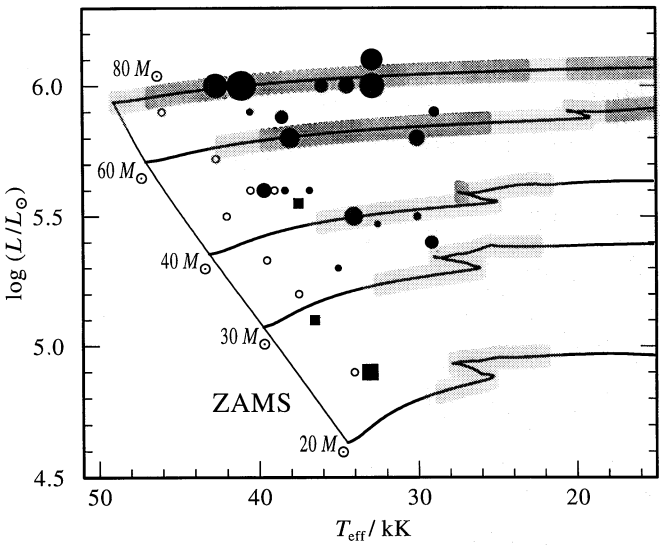

Fig. 3. HR diagram with evolutionary tracks (labels: initial masses) from Kiriakidis et al. (1993). Unstable phases are shaded. Dark shading refers to very unstable phases in which the pulsation growth time is less than 20 times the dynamical time scale. Note that these tracks are conventional in the sense that no additional, pulsation driven mass-loss is accounted for, and are only used here to identify the regions of instability. Superimposed are the observed positions of O stars investigated for optical line profile variations (*lpv*) (from Fullerton 1990, 1991; Fullerton et al., in prep.). The amplitude of variability (see text) is indicated by the size of the filled circles or squares, the latter representing very rapid rotators ($v \sin i > 300$ km s^{-1}). Open circles denote stars with non-variable profiles within detection limits

bility is striking. This holds especially for the hot edge of the instability regime. There are only two exceptions with $\log L/L_\odot < 5.1$, and these are very rapid rotators. Hence, it is evident that objects observed to be variable lie almost exclusively in the theoretical domain of instability. Conversely, the non-variable objects are situated in the regions predicted to be stable. Although a bit speculative at present, this suggests that the observed *lpv* are, directly or indirectly, a consequence of the pulsational mechanism proposed by Kiriakidis et al. (1993).

According to this hypothesis, the pulsations (where the analysis of non-radial components has still to be performed) may be observed directly as *lpv* in the case of less luminous stars, since their "thin" winds contribute negligible to most optical line profiles. In the case of the more luminous objects, which have systematically higher mass-loss rates, optical profiles like He I λ5876 are partly formed in the wind. The *lpv* of these objects usually consist of "bumps" in the profile that progress from lower to higher frequencies, and which are probably due to density enhancements that propagate outwards in the stellar wind. These density enhancements may be connected with the instability arising from the radiation line force (for references see Owocki 1992). If so, they are not direct diagnostics of the pulsations which, however, might be regarded as a trigger mechanism to the line force instability.

The interpretation of the *lpv* observations given above supports the assumptions about the pulsationally enhanced mass-loss made in Sect. 2, since it shows that the predicted pulsations may be real. However, it makes also clear that the occurrence of the strange mode pulsations in itself are not a sufficient criterion for the onset of a Wolf-Rayet type wind. Rather, further conditions must be fulfilled. Note that in Sect. 2 we assumed that the linear growth time of the instability must become sufficiently short in order to yield a significant mass-loss increase.

4. Comparison with observations: LBVs

To further improve our understanding of the evolution of very massive stars, the LBV phase has to be identified and specified within our evolutionary scenario. In more precise terms we refer to this phase as the "P Cygni Type" (brief: PCT) LBV phase (Lamers 1986), which is located close to the Humphreys-Davidson limit at the top of the HR diagram, indicating that VMS do not evolve into red supergiants but turn again into Wolf-Rayet stars after their LBV stage.

4.1. A comparison with the parameters of P Cygni

Among the numerous peculiarities of the atmosphere of P Cygni, two are of special interest here. Firstly, the outbursts which occurred in a phase of major activity in the seventeenth century (Lamers 1986) and secondly, the low stellar mass obtained by application of the radiation-driven wind theory to its quiescent phase (Pauldrach & Puls 1990 – Paper VIII). These two aspects cannot be reproduced by standard stellar evolutionary models. However, the assumption of a violent instability in the stellar envelope at a surface temperature of 20 000 K (see Sect. 2.3) can explain both points. First, the dramatic increase in the mass-loss rate due to this effect (cf. Fig. 2) may correspond to the occurrence of outbursts (note that the position of the instability in the HR diagram coincides with the regime of the PCT-LBVs) and second, owing to the extreme values of the mass-loss rate, the star loses a huge part of its envelope, and hence of its mass, in this phase.

The models of our sequence during shell hydrogen burning (cf. Sect. 2.3) are now compared with the stellar parameters of P Cygni. Let us first adopt, from paper VIII: $\log L/L_\odot = 5.86$, $T_{\rm eff} = 19\,300$ K, $R_* = 76 R_\odot$, and $\log g = 2.04$, implying a mass of $23 M_\odot$. Note that these values were obtained from a consistent modelling of P Cygni with the theory of radiation-driven winds. Independently, the luminosity and the effective temperature are confirmed by a spectroscopic analysis of the H and He lines (see Sect. 4.3), and by a photometric analysis (Lamers et al. 1983). From Figs. 4b,d it is obvious that these values of L and $T_{\rm eff}$ are matched by our track twice on its redward excursion and on the way back. Moreover, Fig. 5 reveals that the surface gravity lies between $\log g = 1.95...2.05$, and hence the mass is almost identical to the value from Paper VIII (compare also with Fig. 4a).

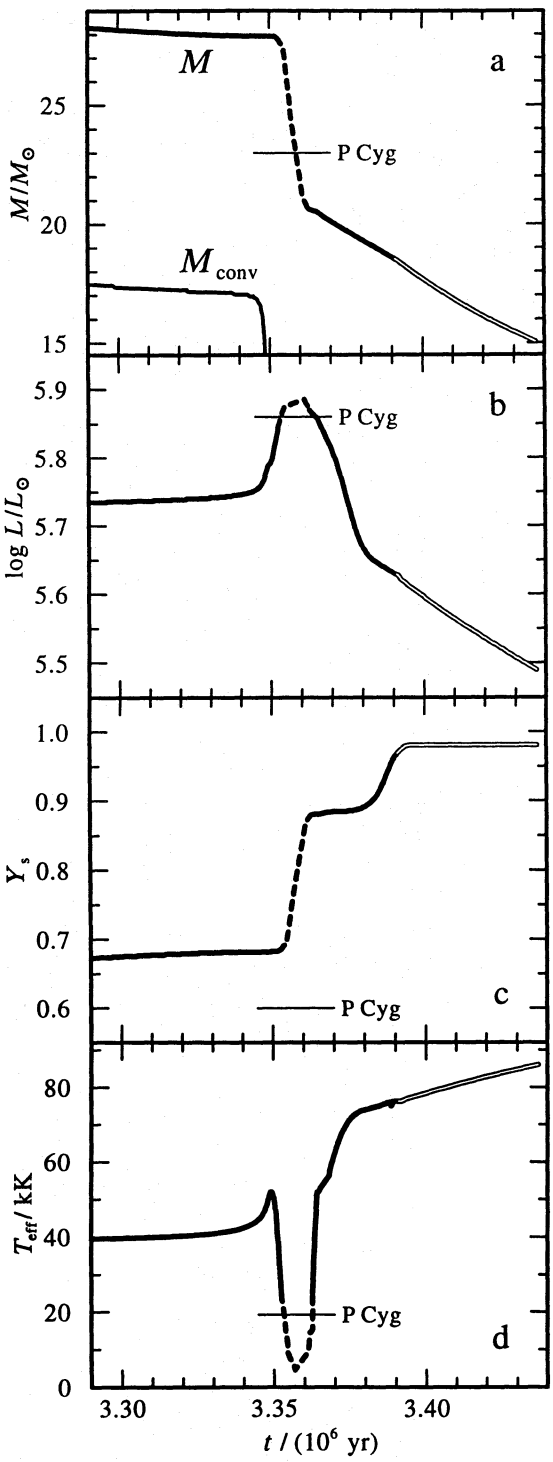

Fig. 4a–d. Various quantities as a function of time from the end of core hydrogen burning through early core helium burning for our $60M_\odot$ computation. **a** Stellar mass and convective core mass. **b** Stellar luminosity. **c** Helium mass fraction at the surface. **d** Effective temperature. The tracks are drawn black as long as hydrogen remains present at the surface ("WNL" stage), but as double line when hydrogen vanishes ("WNE"). The LBV excursion is drawn dashed. The empirical values for P Cygni (see text and Table 4) are indicated

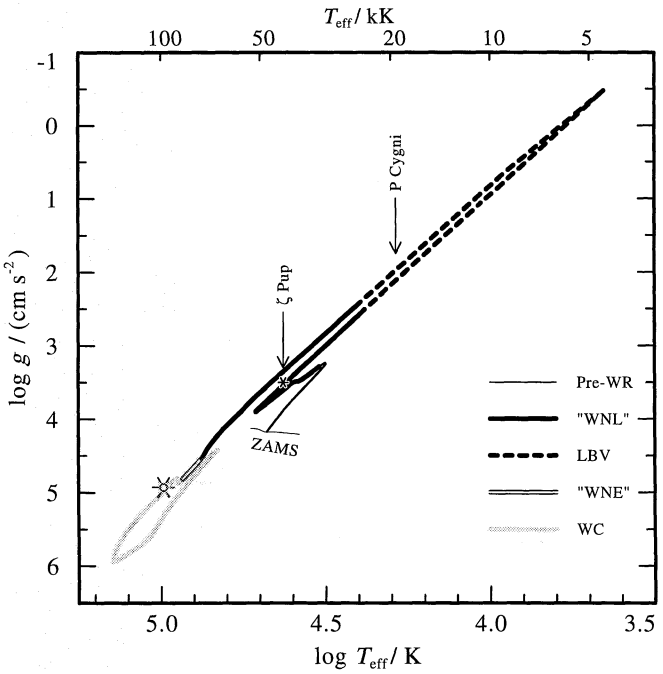

Fig. 5. Gravity (at the effective radius defined consistently with T_{eff}, cf. Sect. 2.1) versus T_{eff} for the $60M_\odot$ track. The evolutionary stages, defined according to the surface composition, are indicated by different drawing styles (see inlet). The adopted effective temperature for P Cygni (19 300 K) and the position of the Of star ζ Puppis are indicated

However, as the present evolutionary models predict a strongly enhanced He abundance for P Cygni[1], the mass determination of Paper VIII is called into question, since the mass of P Cygni has been determined in that paper from adjusting the mass-loss rate predicted by the radiation driven wind theory to the mass-loss rate deduced from the radio flux, and both of these values depend sensitively on the He abundance (in Paper VIII solar abundances have been adopted and a mass-loss rate $\dot{M}_{radio} = (12.1 \pm 3.5)10^{-6} M_\odot$ yr^{-1} was derived).

Thus both results from Paper VIII, the mass and the mass-loss rate, must be possibly corrected, since due to the larger helium abundance less electrons are available per atomic mass unit. We will show in the following subsections that a value of $\dot{M} = (35.0 \pm 7.0)10^{-6} M_\odot$ yr^{-1} is consistent with the radiation-driven wind model, the analysis of the line spectrum, and the observed radio flux.

Because the ratio of the local electron density, $n_e(r)$ to the particle density, $\rho(r)$ drops significantly with increasing helium abundance, the radiative acceleration due to Thomson scattering decreases. Hence, the ratio of stellar to Eddington luminosity

$$\Gamma(r) = 3.04\ 10^{-5} \frac{n_e(r)}{\rho(r)\, m_H} \frac{L}{L_\odot} \frac{M}{M_\odot} \qquad (4)$$

[1] Figure 4c indicates a helium mass fraction Y_s in the range from 0.67 to 0.84, corresponding to a number ratio of $n_{He}/n_H = 0.54...1.5$; a strong enhancement of helium is also confirmed by the spectroscopic analysis (see below, Sect. 4.3)

Table 2. Radiation driven wind models for P Cygni. The resulting mass-loss rate $\dot{M}$, the ratio of actual to Eddington luminosity Γ, and the ratio of the mass-loss rate to the terminal wind velocity are given in dependence from the helium abundance, which is quoted alternatively as number ratio $n_{\rm He}/n_{\rm H}$ and as mass fraction $Y_{\rm s}$. The stellar mass is always adopted as 23 $M_\odot$.

$n_{\rm He}/n_{\rm H}$	$Y_{\rm s}$	$\dot{M}$ $M_\odot\,{\rm yr}^{-1}$	Γ	$\dot{M}/v_\infty$ $M_\odot\,{\rm yr}^{-1}/({\rm km\ s}^{-1})$
1.5	0.84	$17.8\,10^{-6}$	0.34	$4.5\,10^{-8}$
1.0	0.78	$20.6\,10^{-6}$	0.38	$6.9\,10^{-8}$
0.75	0.74	$25.4\,10^{-6}$	0.43	$8.0\,10^{-8}$
0.54	0.67	$34.7\,10^{-6}$	0.47	$10.2\,10^{-8}$

becomes much smaller than unity (while a value of $\Gamma = 0.78$ was obtained in Paper VIII for the stellar parameters given above at the sonic point, $\Gamma = 0.47$ is now found for $n_{\rm He}/n_{\rm H} = 0.54$, and $\Gamma = 0.34$ for $n_{\rm He}/n_{\rm H} = 1.5$). Although P Cygni now appears to be a factor of two further away from the Eddington limit, and although the observed mass-loss rate is a factor of three larger than thought before, it can nevertheless be reproduced by models which represent the state of the art of the theory of radiation driven winds (cf. Pauldrach et al. 1994a, Paper XII; Pauldrach et al. 1994b). This is due to the considerable recent improvement of the atomic data, as will be shown in the following subsection.

4.2. New radiation-driven wind models for P Cygni

The adequate modeling of P Cygni's wind requires accurate and complete atomic data for the most important ionization stages. Since we know from previous calculations (Paper VIII) that up to 76% of the total line force is provided by elements of the iron group in ionization stages III and II, we concentrated on these. To implement the improved atomic models for Fe III, Cr III and Ni III we utilized the method described in Paper XII, whereas the energy levels and the line transitions from the Kurucz (1992) compilation have been used for Fe II, Cr II, Ti II, Ti III, Mn II, Mn III, Co II, Co III and Ni II. For the calculation of the line force these new atomic models provide a factor of ten more spectral lines (almost 10^6 lines are taken into account) than the simplified atomic models used in Paper VIII. The Grotrian diagram for the Fe III model ion, one of the most important ions for the line force in the wind of P Cygni, is shown in Fig. 6 as an example. Test calculations showed that this much larger number of lines gives rise to an enhancement of the radiative line acceleration ($g_{\rm line}$ increases by more than a factor of 2), which over-compensates for the loss of acceleration due to Thomson scattering. 90% of the total line force is now provided by elements of the iron group; the most important ionization stages in order of their maximum contribution to the line force are Fe III (56%), Cr III (27%), Mn III (10%), Ni III, Co III, Ti III and Ni II, Mn II, Fe II.

In view of this promising result, we perform wind calculations for a model grid of stellar parameters. The grid is based on the well established values $T_{\rm eff}$ = 19 300 K and

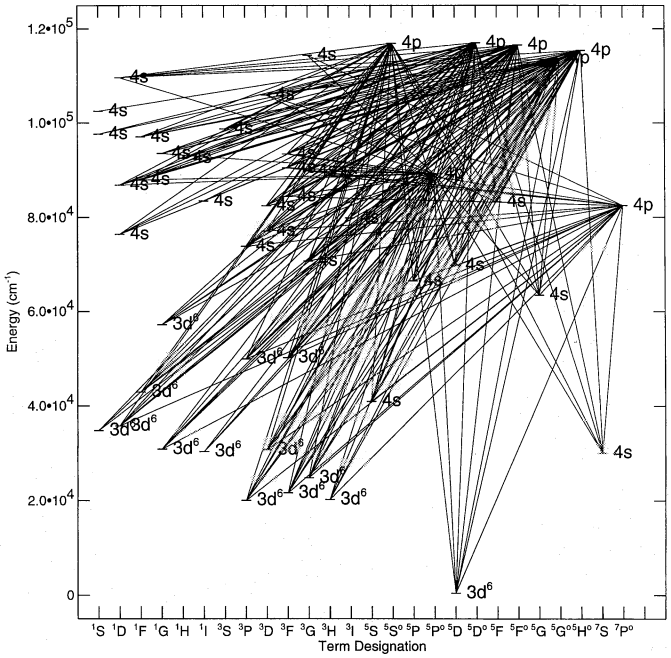

Fig. 6. Grotrian diagram of Fe III describing the corresponding model ion as used in our radiation driven wind models for P Cygni

$\log L/L_\odot = 5.86$, Fixing first the mass at the value obtained in Paper VIII ($M = 23 M_\odot$), we varied the helium abundance in the range indicated by our evolutionary track (cf. Fig. 4c). The results of these calculations are shown in Table 2. It is readily seen that $\dot{M}$ increases strongly with decreasing helium abundance and that at, or somewhat below, the lower limit of $n_{\rm He}/n_{\rm H} = 0.54$ the mass-loss rate $\dot{M} = (35.0 \pm 7.0)10^{-6} M_\odot\,{\rm yr}^{-1}$ postulated in Sect. 4.1 is reached.

On the basis of this result we now fix the He abundance at $n_{\rm He}/n_{\rm H} = 0.54$ ($Y_{\rm s} = 0.67$) and carry out a second set of calculations by varying now the mass around $23 M_\odot$. Table 3 displays the results. Most surprisingly, these calculations show the same discontinuity in $\dot{M}$ — more pronounced in the ratio $\dot{M}/v_\infty$ (note that this value is directly proportional to the density) — as was found in Paper VIII in exactly the same range of surface gravity ($\Delta \log g < 0.2$) and mass. By comparing the calculated and observed mass-loss rates, it is further confirmed that P Cygni's mass ($M = 23 M_\odot$) coincides precisely with the regime of the bi-stability. We can thus reproduce not only the dynamical properties of P Cygni's wind during quiescence and determine the mass from that, we can also confirm our earlier suggestion that the shell ejection, i.e. the wind variability during quiescence, occurs on the basis of the feed-back mechanism of the bi-stability (cf. Paper VIII).

However, there is observational evidence that a density increase of a factor of 5 has to be assumed for a shell (Waters & Wesselius 1986; see also van Gent & Lamers 1986; Lamers 1986; van den Oord et al. 1985). In view of our calculations this can only be achieved if P Cygni's quiescent phase is located just at the discontinuity, since in this case a jump across the

Table 3. Radiation driven wind models for P Cygni as a function of the adopted stellar mass (cf. also Table 2). The helium abundance is now fixed at $n_{He}/n_H = 0.54$ ($Y_s = 0.67$).

M $M_\odot$	$\log g$ cgs	$\dot{M}$ $M_\odot\,yr^{-1}$	Γ	$\dot{M}/v_\infty$ $M_\odot\,yr^{-1}/(km\,s^{-1})$	$\frac{v_\infty}{v_{esc}}$
28.0	2.13	$16.8\,10^{-6}$	0.38	$3.5\,10^{-8}$	1.59
23.0	2.03	$34.7\,10^{-6}$	0.47	$10.2\,10^{-8}$	1.38
19.0	1.9	$48.9\,10^{-6}$	0.57	$17.1\,10^{-8}$	1.40

discontinuity, producing the shells (cf. Paper VIII), increases $\rho \sim \dot{M}/v_\infty$ by almost the correct factor. This would, however, require that the observed mass-loss rate be reproduced before the jump across the discontinuity occurs. From Table 2 it is obvious that this can only be achieved for a helium abundance somewhat smaller than $n_{He}/n_H = 0.54$ ($Y_s = 0.67$).

Hence we find that the stellar parameters from our evolutionary calculations and those from radiation driven wind models are consistent. Even the helium abundance is compatible, if the smallest value from the beginning of the LBV phase (cf. Fig. 4c) is adopted. This implies that P Cygni may be at the beginning of its LBV excursion, in agreement with its observed visual brightening over the last centuries which indicates that this star is rapidly evolving towards higher temperatures, as shown by de Groot & Lamers (1992). They estimated the rate at which the effective temperature of P Cygni changes with time to be $6 \pm 1\%$ per century which compares well with the 5.8% per century change of our model around $T_{eff} \simeq 20\,000$ K. Since our scenario predicts a rapidly increasing He abundance for P Cygni, we anticipate that its mass-loss rate will significantly decrease within the next centuries.

4.3. Constraints from the spectrum of P Cygni

Stellar parameters of P Cygni can in principle be determined from a detailed spectroscopic analysis. Using the non-LTE method presented by Hillier (1987, 1990) we have performed a parameter space investigation (Najarro et al. in prep.) with the observational constraints given by the averaged optical and near–IR spectra obtained by Stahl et al. (1993). The models account for the radiative transfer in spherically expanding atmospheres, subject to the constraints of statistical and radiative equilibrium. Steady state is assumed, and the density structure is set by the mass-loss rate and velocity field via the equation of continuity. The transfer equation is solved using either the Sobolev approximation, corrected for the diffuse radiation field (Hillier 1987), or by means of an accurate solution of the comoving-frame transfer equation. We account for a pure H–He composition with 15 H, 49 He I ($n \leq 10$) and 7 He II levels in the model atoms.

Table 4 shows the model parameters which reproduce best the hydrogen lines (Hα, Hβ, Hγ, P_{11} and P_{12}) as well as the main optical He I lines. The obtained stellar radius and effective temperature (and hence stellar luminosity) agree with those

Table 4. Stellar parameters of P Cygni obtained from a detailed spectroscopic analysis.

R_* $R_\odot$	T_{eff} kK	$\log L/L_\odot$	n_{He}/n_H	$\dot{M}$ $M_\odot\,yr^{-1}$	v_∞ $km\,s^{-1}$
76	19.3	5.86	0.4	$3.35\,10^{-5}$	185

from previous works (Lamers et al. 1983, Paper VIII) and fit our evolutionary model as shown in Fig. 4. Moreover, the enhanced helium abundance ($n_{He}/n_H = 0.4$, corresponding to $Y_s = 0.60$) confirms the result of Sect. 4.2. Essentially, P Cygni's helium abundance is well constrained by the optical He I profiles and their ratios to the hydrogen lines. We found $n_{He}/n_H = 0.55$ and $n_{He}/n_H = 0.3$ as reasonable upper and lower limits, respectively – a similar helium abundance ($n_{He}/n_H = 0.5$) has been obtained by Deacon & Barlow (1991) from JHKL spectra.

The mass-loss rate we obtain from our spectral analysis is considerably higher than previous estimates from the radio flux (cf. van den Oord et al. 1985). However, both methods depend critically on the helium abundance and the ionization structure of the wind.

4.3.1. The ionization structure in the wind of P Cygni

It is crucial to note the sensitivity of the wind ionization structure to changes in the stellar luminosity and mass-loss rate, and its connection with the interpretation of P Cygni's wind bi-stability (Paper VIII). Our model parameters place the star in a regime where H and He start to recombine far out in the wind. However, an increase of only 0.05 dex in luminosity (500 K in T_{eff}) would force both species to be ionized throughout the whole wind. Alternatively, if the wind is ionized and $\dot{M}$ is increased, e.g, by shell ejection, the radiation field is not able to keep the denser wind ionized, and H and He will start to recombine. Further, if recombination does take place in the wind, it will significantly reduce the emergent flux at those wavelengths where the continuum formation occurs in the outer wind, i.e., in the sub-millimeter and radio range, and thus explain the enhanced observed variability in the radio region.

The wind ionization structure is reflected in the shape of the line profiles. Although the He I profiles can be equally well fitted by both, "ionized" and "recombined" models, the absorption dips of the Balmer lines can be reproduced only in the recombined case. The reason for that behavior may be explained as follows. If H recombines in the wind, it causes an increase of the optical depth in Lα, which leads to an overpopulation of the second level of H and, hence, a significant increment in the opacity of the Balmer lines. When H is ionized throughout the whole wind, Lα becomes optically thin in the wind and we recover the case of pure recombination emission line profile. This effect is shown in Fig. 7, where computed Hα profiles for both types of models are plotted and compared with the observation.

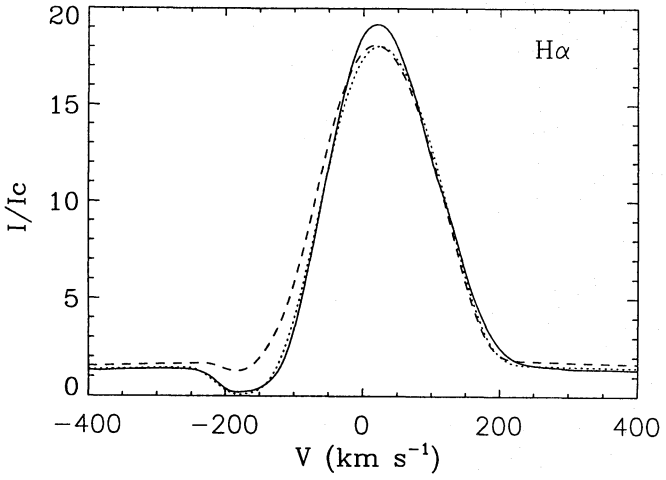

Fig. 7. Comparison of the observed Hα line of P Cygni (solid line) with theoretical profiles from two alternative models with a "recombined" (dotted) or "ionized" (dashed) wind structure (see text)

Our preference for the "recombined" model explains why we obtain now a larger mass-loss rate compared to previous studies. Moreover, since the enhanced helium abundance, together with the recombination, significantly reduces the density of electrons and ions in the wind, this higher mass-loss rate is consistent with the observed radio free-free emission.

4.4. Other P Cygni type LBVs and Ofpe/WN9 stars

Similar spectral characteristics as shown by P Cygni are found in some other LBVs and Ofpe/WN9 stars. The infrared spectra of a dozen of Galactic broad emission line stars, reported by McGregor et al. (1988a), together with the discovery of a cluster of He I emission line stars in the Galactic Center (Krabbe et al. 1991), represent a significant step towards populating the observational gap between the evolutionary O and WR phases. Detailed spectroscopic analyses of the Galactic Center objects (Najarro et al. 1994; Genzel et al. 1994) indicate a highly evolved status ($n_{\rm He}/n_{\rm H} > 1$), and classify these objects as Ofpe/WN9 stars, similar to those observed in the Magellanic Clouds (McGregor et al. 1988b).

The ratios between the infrared He and H line strengths observed by McGregor et al. (1988a) in Galactic emission line stars indicate a big scatter in the helium abundances, although quantitative determinations are still lacking. Recently, Smith et al. (1994) have performed tailored analyses for two of these objects: AG Car and He 3-519. Both objects present stellar luminosities and helium abundances close to those we have obtained for P Cygni (cf. also Leitherer et al. 1994; Davidson et al. 1994). Similar stellar parameters were obtained for the Galactic WN9 star WR 108 (Schmutz et al. 1989; Hamann et al. 1993; Crowther et al. 1994) although it shows a faster wind. The positions of these objects are included in Fig 9. Future He abundance determinations for the other Galactic broad line emission line stars will certainly give invaluable insight into this short but extremely interesting phase of stellar evolution.

5. Comparison with observations: Wolf-Rayet stars

5.1. Mass-loss rates

In our scenario the strong mass-loss observed for WR stars is a direct consequence of the suggested stellar pulsations. In this respect, it may reveal also the solution for the still unsolved problem of the *different* behavior of O star and WR star winds. Briefly, the present situation is as follows: for O stars, both the mass-loss and its acceleration are primarily controlled by radiation pressure (for recent results and references, see Paper XII), where the obtained ratio of wind momentum to the momentum of the stellar radiation field, the so-called "performance number" $\eta = \dot{M} v_\infty/(L/c)$ is typically smaller than unity. On the other hand, the "observed" values of η for WR winds are much larger (e.g. Hamann et al. 1993). Recently, however, Lucy & Abbott (1993) showed that significantly high performance numbers of $\eta \lesssim 15$ can be actually obtained by *multi-scattering* processes, *if a large value for $\dot{M}$ is adopted to be present.* This different behavior compared to O star winds (cf. Puls 1987) originates from the fact that in a wind with a high $\dot{M}$ the ionization balance gets a steep gradient with respect to radius (cf. Hillier 1989; Hamann et al. 1992, 1993) — in contrast to O stars where the ionization balance remains more or less constant. Hence, a photon on its way through the wind can be processed by much more lines (resulting from higher ionization stages inside and lower stages outside) than it would experience in the case of O star winds. Thus, the "effectivity" of the multi-scattering process is largely enhanced. (For a detailed investigation of this process as function of line density, cf. Springmann 1994.)

This result, however, does *not* explain the principal difference between O-type and WR-type winds, because the large $\dot{M}$ in WR winds is required *a priori* to initiate the process. If one would allow the $\dot{M}$ to be fixed by line pressure only, the resulting value would be comparable to rates found for O stars (for scaling relations see Pauldrach et al. 1986), unless the WR is situated (unrealistically) close to the Eddington limit (cf. Pauldrach et al. 1985; Friend et al. 1987).

Although it cannot be excluded that a certain part of the acceleration required to lift the matter beyond the sonic point will be additionally provided by bound-free/free-free continuum acceleration which is not yet accounted for in the radiation driven wind models (cf. Puls & Pauldrach 1991; Pauldrach et al. 1994b), the mechanism suggested here leads to an easy understanding of the different behavior: since the mass-loss in WR stars is now lifted beyond the sonic point by an *internal* mechanism (the pulsations!), it can no longer be modified in the supersonic part ("stellar wind laws", Holzer 1977) and is intrinsic to the wind. Thus, it may be actually accelerated by multiple scattering and exhibit the observed large performance numbers.

5.2. HRD positions

Recent progress in the modeling of non-LTE radiation transfer in expanding atmospheres now allows for the quantitative analysis of Wolf-Rayet spectra (for a recent review, see Hamann

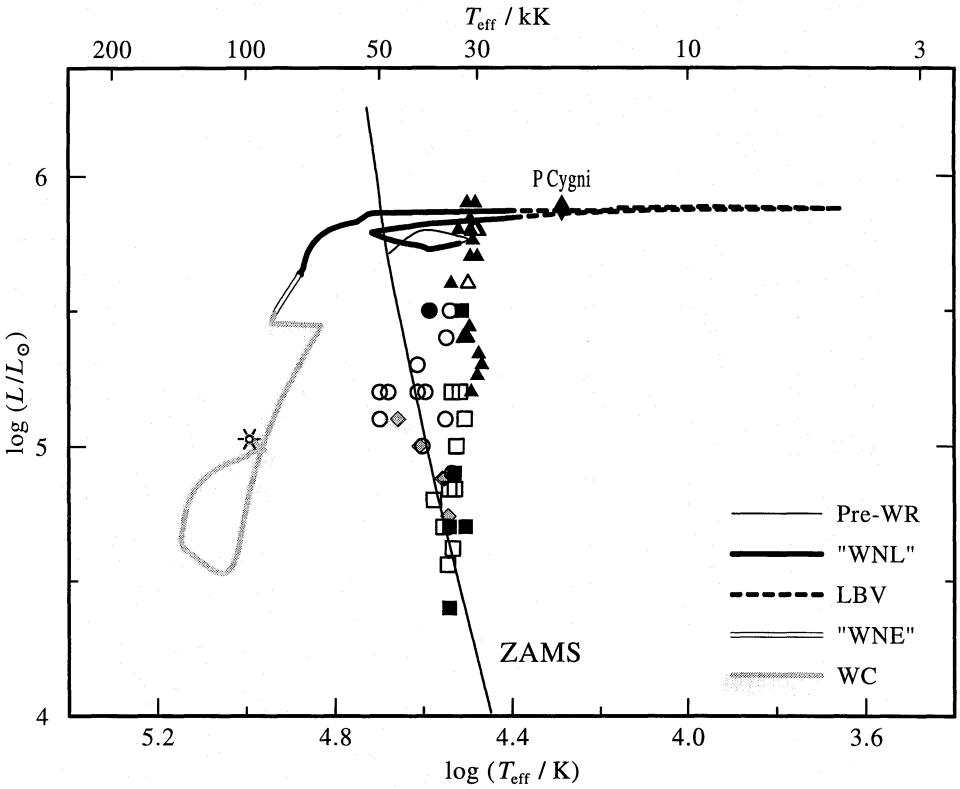

Fig. 8. Hertzsprung-Russell diagram. Discrete symbols indicate the locations of the Galactic WR stars as obtained from spectral analyses. Triangles, circles or squares refer to WNL, WNE-s or WNE-w stars, respectively, while filled or open style indicates whether hydrogen has been detected or not. WC stars are represented by shaded diamonds. The black diamond indicates the luminous blue variable star P Cygni. Superimposed is the theoretical evolutionary track described in Sect. 2. The evolutionary stages, defined according to the surface composition, are indicated by different drawing styles (see inlet). Note that the subclass definitions "WNL" and "WNE" used here refer to the presence or absence of hydrogen at the surface and thus can be directly compared with the representation of the observed stars by filled or open symbols. The effective temperature used as abscissa refers to the "effective radius" (Rosseland optical depth of 2/3) in all cases

1994). The vast majority of the Galactic WN stars has been analyzed so far (Hamann et al. 1993) with respect to their basic parameters. Corresponding work on WC stars is in progress (Koesterke 1993; Koesterke et al., in preparation).

The observed positions in the HRD are compared to the evolutionary track in Fig. 8. Discrete symbols indicate the locations of the Galactic WR stars as obtained from spectral analyses. Triangles, circles or squares refer to WNL, WNE-s or WNE-w stars, respectively[2], while filled or open symbols indicate whether a detectable amount of hydrogen is present in their atmosphere or not. WC stars are presented by shaded diamonds. The black diamond indicates the luminous blue variable star P Cygni (Najarro, in preparation). Superimposed is the theoretical evolutionary track described in Sect. 2 (f = 1). The evolutionary stages, defined according to the surface composition, are indicated by different drawing styles (see inlet). Note that the subclass definitions "WNL" and "WNE" used here refer to the presence or absence of hydrogen at the surface[3] and thus can be directly compared with the representation of the observed stars by filled or open symbols, respectively.

The two "WNL" phases of the evolutionary track fall into the region of the most luminous observed WNL stars with hydrogen. Note that the LBV excursion meets the position of P Cygni. A favorable feature of the presented track is the significant decrease of the luminosity before and during the "WNE" stage, as the hydrogen-free WN stars are indeed observed to be less luminous. A similar track with a lower initial mass (e.g. 40 $M_\odot$) might match the observed WN stars with lower luminosities. Note that the initial masses required for a given WN luminosity are somewhat lower for the type of tracks presented here than for the standard evolution. Nevertheless, the least-luminous WN stars probably need a different explanation, and are possibly formed by close-binary evolution (for an overview see, e.g., Vanbeveren 1991). Indeed, the WR component of the WN5+O6 binary V444 Cygni is located in the HRD just among

[2] Among the WN spectra, one distinguishes between "late" (WNL) and "early" (WNE) subtypes according to the relative strengths of N and He lines from different ionization stages. The designation WNE-s or WNE-w is given to WNE stars with strong or weak lines, respectively.

[3] In the context of evolutionary calculations, "WNL" or "WNE" means phases in which hydrogen is present or absent at the surface, respectively. The quotation marks shall distinguish these terms from the spectroscopic classification.

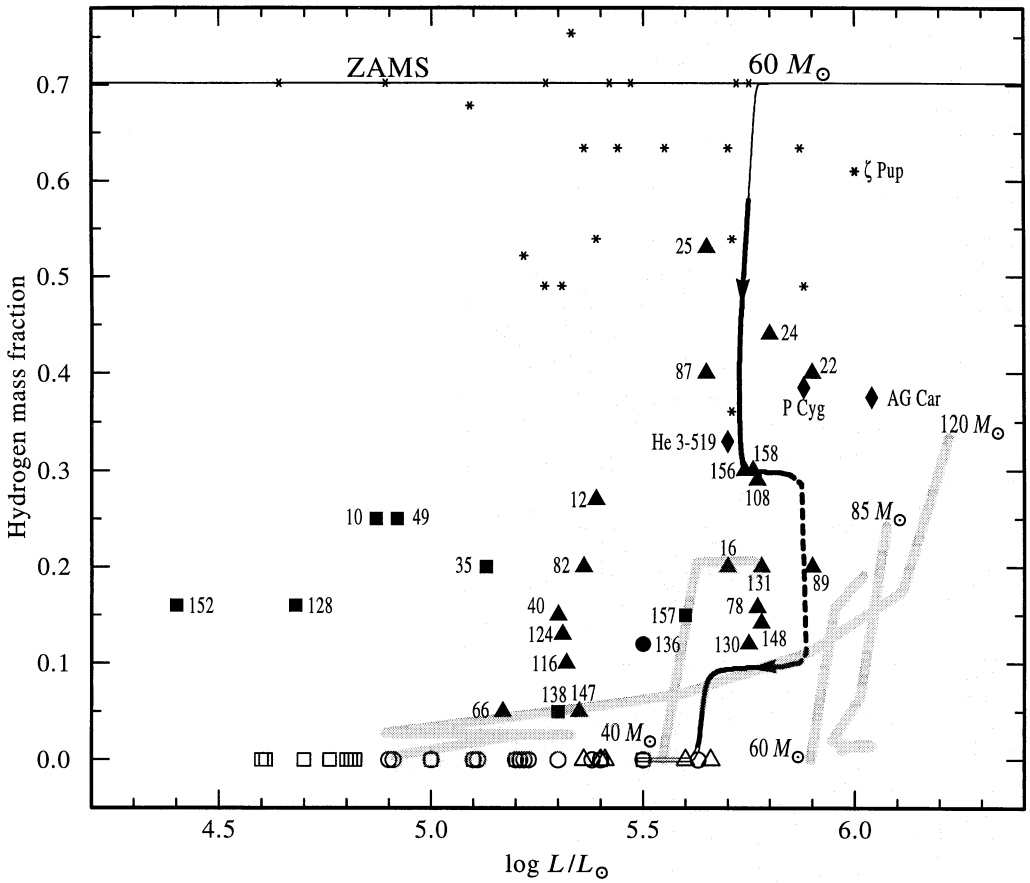

Fig. 9. Hydrogen abundance versus luminosity for Galactic WN stars (labels: WR numbers according to the catalog by van der Hucht et al. 1981). Triangles, circles or squares refer to the different spectral types WNL, WNE-s or WNE-w, respectively. Open symbols crowding at zero hydrogen abundance indicate the luminosities of those WN stars showing no hydrogen signature. Small asterisks mark Galactic luminous OB stars analyzed by Herrero et al. (1992), only ζ Puppis being individually labeled. Black diamonds indicate the three LBVs analyzed so far (P Cygni: Najarro et al. in preparation; AG Car and He 3-519: Crowther & Willis 1994; Smith et al. 1994). The shaded lines give the hydrogen abundances for the "WNL" phase as predicted by the evolutionary calculations with high mass loss rates of Meynet et al. (1994), for $Z = 0.02$ and initial masses as indicated. The new evolutionary track presented in this paper is also shown; different drawing styles (cf. Fig. 8) refer to the predicted spectral appearance as "WNL" (heavy line), LBV (dashed), again "WNL" and finally "WNE" (double line)

the group of WN stars with lowest luminosities (Hamann & Schwarz 1992). During the WC phase the evolutionary track passes through the observed luminosity range.

Quoting effective temperatures of WR stars is not straightforward due to the spherical extension of their atmospheres. Contrary to the case of "normal" plane-parallel atmospheres, the definition of an effective temperature here depends on the choice of a reference radius $R_{\rm eff}$ ($L = 4\pi R_{\rm eff}^2 \sigma T_{\rm eff}^4$, with L being the well-defined quantity). Only the optically thin part of the atmosphere can be seen from the outside, and therefore we have chosen the "observable" $T_{\rm eff}$ as referring to the radius $R_{\rm eff}$ of radial optical depth 2/3 (Rosseland mean) for the representation of the empirical data in the HRD (Fig. 8). The same choice was made for the evolutionary track (cf. Sect. 2.1), but in this case the values obtained for $R_{\rm eff}$ and thus for $T_{\rm eff}$ depend on the velocity law adopted for the optically thick part of stellar wind, which is principally unobservable. Thus any discrepancy between predicted and observed $T_{\rm eff}$ might only indicate that the sub-photospheric, but non-static layers are more (or less) extended than implied by the ad-hoc assumptions in the evolutionary models.

However, it is worth noting that the effective temperatures of our hydrogen-rich WN models are almost unaffected by these assumptions (i.e. by the choice of β, v_∞, and $\kappa_{\rm wind}$; cf. Sect. 2.1) due to the still relatively small optical depth of the wind layers ($\tau_{\rm wind} \lesssim 1$). Consequently, a comparison of their temperatures with observations is meaningful. The agreement of the effective temperatures of these models with that of the observed luminous WNL stars (see Fig. 8) thus indicates that the temperature range for which strong pulsational instabilities are found (cf. Fig. 1) coincides with the observed WNL temperatures. This finding confirms the self-consistency of our model sequence and supports our assumption that the strong pulsationally instability results in a Wolf-Rayet type stellar wind.

5.3. Abundances

The empirically determined hydrogen abundances are plotted in Fig. 9 versus the luminosity for Galactic WN stars. The hydrogen abundances are from analyses by Hamann et al. (in preparation), Crowther et al. (private communication), or Hamann et al. (1991). These hydrogen mass fractions have typical error margins of about ± 0.05. The luminosities are throughout from Hamann et al. (1993). Open symbols crowding at zero hydrogen abundance indicate the luminosities of those WN stars showing no hydrogen signature in their H I-Balmer/He II-Pickering decrement (also after Hamann et al. 1993). The results form a significant, unexpected pattern. Below a luminosity of $10^{5.6}\,L_\odot$ one finds only hydrogen abundances in the range of about 0.25 ... 0 (by mass). Above $10^{5.7}\,L_\odot$ there exist no hydrogen-free WN atmospheres at all. Instead, the observed hydrogen mass fractions for these luminous WN stars range from 0.12 to 0.5 .

The track corresponding to our scenario is also shown in Fig. 9, using the same drawing styles as introduced in the HRD (cf. inlet of Fig. 8). The first "WNL" phase could be identified with the group of WNL stars having the highest hydrogen mass fraction left (WR 25, WR 22 ...). Then the LBV stage and a second "WNL" phase are predicted to follow while the evolution proceeds with decreasing hydrogen surface abundance. This agrees qualitatively with the observed location of P Cygni and the second group of luminous WNL stars (WR 158, WR 156, WR 108 ...), but quantitatively the observed hydrogen abundances are higher than predicted. The decreasing luminosity during the second "WNL" phase can explain the observed lack of zero-hydrogen counterparts with $L > 10^{5.7}\,L_\odot$. However, the formation of WN stars with, say, $L < 10^{5.4}\,L_\odot$ requires different tracks, either with smaller initial mass or within a different scenario.

The shaded lines in Fig. 9 indicate the hydrogen abundance during the "WNL" phase as predicted by the evolutionary calculations of Meynet et al. (1994). These tracks agree well with the hydrogen-poor ($X_s = 0.2...0.1$) luminous WNL stars, and the $120 M_\odot$ track even accounts for the group WR 66, WR 138 and WR 147 (cf. Fig. 9). However, too luminous H-free WN stars are predicted, and no H-rich ($X_s \gtrsim 0.3$) WNL stars are produced (cf. Sect. 6).

The existing spectral analyses of the composition of WC atmospheres confirm that this material was partly processed by the 3α-reaction. The intermediate subtypes (WC5-7) analyzed so far by means of stratified models (Hamann et al. 1992; Koesterke 1993; Koesterke et al., in preparation) show carbon-to-helium ratios between 0.25 and 1.5 (by mass), which is in the range predicted by both the standard evolutionary models and the alternative track presented here.

6. Discussion

The assumption of pulsationally enhanced mass-loss for evolved main sequence stars used in the present calculations is qualitatively new and leads to qualitatively new results, while the quantitative description of this process is certainly preliminary. Therefore, a quantitative agreement of our track with observations may not be anticipated, but any comparison should focus on qualitative aspects. However, quantitative discrepancies are worth considering since they may provide a guideline for further improvements of the quantitative description.

In Sect. 3 we have seen that in fact the variability observed in O stars increases with decreasing surface temperature and increasing luminosity (cf. Fig. 3), as expected from the linear pulsation study of Kiriakidis et al. (1993). We have argued in Sect. 5 that the increased mass-loss rates of Wolf-Rayet stars require a mechanism in addition to radiative acceleration at least to initiate the dense outflow. Lamers & Leitherer (1993) pointed out that the performance number η increases along the spectral sequence from O to WNL stars. This — in our picture — may correspond to the onset of the effect of pulsations with decreasing effective temperature, which, in turn, is related to the growing strength of the pulsational instability (see Kiriakidis et al. 1993). Let us mention here, that also the mass-loss rates of hydrogen-free WR stars are consistent with this picture: Glatzel et al. (1993) have found that massive helium stars suffer from the same type of instability as the very massive main sequence stars. They found a lower mass limit for the occurrence of the instability of $\sim 4 M_\odot$, which fits very well to the observed lower luminosity limit of Wolf-Rayet stars of $\log L/L_\odot \simeq 4.5$ (cf. Langer 1989a). Furthermore, they predict the instability to increase with the mass of the helium stars, which is well in line with the semi-empirical mass dependent WR mass-loss rate used for our calculations (cf. Sect. 2.4).

Within this picture, the spectral sequence O → hydrogen-rich WNL reflects mainly the increase in the mass-loss rate. That this is also an evolutionary sequence can be concluded from the fact that the surface helium abundance increases along this sequence (cf. Fig. 9). In this context our theoretical track has the following problem: an increased helium abundance is found only rather late in the evolution, i.e. at a time where the mass-loss rate is already as large as $\sim 3\,10^{-5} M_\odot\,\mathrm{yr}^{-1}$. Thus, our sequence contains models with initial surface composition but mass-loss rates which are typical for Wolf-Rayet stars, but not for O stars. On the other side, the observations yield the following picture: WN stars with a solar surface composition apparently do not exist (Hamann et al. 1993). However, hydrogen mass fractions as large as 50% are found in luminous WNL stars (cf. Fig. 9). It is remarkable that such a composition can also be found in several O stars (Herrero et al. 1992, cf. Fig. 9). It is therefore possible that internal mixing processes in massive stars increase the surface helium abundance well before they enter the pulsational instability regime. A theoretical study including these mixing processes (cf. Maeder 1987; Langer 1992) has to be left for future investigations. However, let us point out that our sequence also predicts a long-lasting ($9\,10^5$ yr) phase of large (WR-type) mass-loss rates ($\dot{M} \gtrsim 10^{-5} M_\odot\,\mathrm{yr}^{-1}$) and considerable surface helium enrichment ($Y_s = 0.3...0.7$); cf. Table 1. Accordingly, we tend to identify the hydrogen-rich late-type WN stars to be in the core hydrogen burning phase of evolution.

Another qualitative prediction of our model is that hydrogen-rich WNL stars may evolve into PCT-LBVs. In Sect. 4 we have shown that the hydrogen shell burning models of our sequence do correspond in many respects to the prototype star P Cygni. This is particularly supported by the small mass of P Cygni, and by its strong helium enrichment. Quantitatively, the helium content of our H-shell burning models ($Y_s \gtrsim 0.7$) appears to be somewhat too large in order to exactly match the value of P Cygni ($Y_s \lesssim 0.6$; cf. Fig. 9) or to perfectly fit to the values found for other PCT-LBVs ($\sim 0.6 - 0.7$; cf. Smith et al. 1994). However, it matches the qualitative aspect that hydrogen-rich WNL stars are found to have larger hydrogen abundances than PCT-LBVs (cf. Fig. 9, and Crowther et al. 1994), which — since both types of stars have similar luminosities — strongly supports the evolutionary sequence as H-rich WNL → LBV. We want to point out here that Walborn (1989, and priv. communication) has already proposed that the most luminous WNL stars may evolve into LBVs (rather than vice versa) for purely observational reasons.

A further qualitative feature of our track is the prediction of a second, hydrogen-poor post-LBV "WNL" stage. The hydrogen mass fraction in that stage is ~10% in our model. In comparing this feature with observations (cf. Sect. 5, and Fig. 9) we find again that the qualitative behavior agrees well, i.e. "WNL" stars with hydrogen abundances smaller than those found in PCT-LBVs are observed. However, also in this case the quantitative agreement is not perfect.

Actually, our sequence would fit quantitatively better to the observations when the LBV phase would be shifted upwards to somewhat larger hydrogen abundances in Fig. 9. This could be achieved by slightly reducing the f-parameter in Eqs. (1) and (2), i.e. by a slight reduction of the pulsationally induced mass-loss, and by an earlier termination of the LBV mass-loss (cf. Sect. 2.3). It is remarkable that this correction would not only increase the surface hydrogen abundance in the second "WNL"-phase, but also significantly increase its life time, which — in our calculation — appears uncomfortably short in view of the relatively large number of observed post-LBV "WNL" stars (cf. Fig. 9). However, note that the life time of our H-poor "WNL" phase is also directly proportional to the inverse of the mass-loss rate adopted for this phase, which is not very well determined.

Finally, note the sharp decline in luminosity during the hydrogen-poor "WNL" phase in Figs. 8 and 9, which is a particular feature of our sequence and a direct consequence of the previous mass-loss history. Due to this decline one avoids predicting hydrogen-free "WNE" stars with luminosities exceeding the observed upper luminosity limit for those stars. It is important that only increased mass-loss *during the core hydrogen burning phase* of evolution has the effect of lowering the luminosity in the early "WNE" phase, since e.g. an increased LBV mass-loss would not reduce the size of the helium core.

Despite the remaining problems when comparing our models with observations, our track matches several qualitative aspects much better than evolutionary sequences existing in the literature. Let us confront our track with the $60 M_\odot$ sequence at $Z = 0.02$ of Schaller et al. (1992), who adopted a moderate amount of convective core overshooting and — more important — did not incorporate any effects of pulsations (which had not been discovered at that time). Their track does not show any surface enrichment throughout the main sequence evolution, and does not experience extreme mass-loss during that phase. Thus, in the ensuing adopted LBV phase, the stellar mass decreased from $48 M_\odot$ to $34 M_\odot$, and the surface hydrogen mass fraction decreased from its initial value of $X_s = 0.68$ to $X_s = 0.20$. Consequently, no (core-H burning) pre-LBV "WNL" stars are obtained by them, and the observed luminous hydrogen-rich WNL stars are not explained. Furthermore, the characteristics of PCT-LBVs are missed: their low mass (or large L/M ratio) is not obtained (cf. also El Eid & Hartmann 1993), and their highly enriched surface composition is hard to understand: the observed range of $Y_s \simeq 0.6 - 0.7$ is in the range of the LBV models of Schaller et al.; however, also LBVs with cosmic composition ($Y_s \simeq 0.30$) should exist, which seems not to be the case. Finally, the sequences of Schaller et al. largely violates the observed upper luminosity limit for hydrogen-free WN stars.

Some of the problems quoted above are discussed by Meynet et al. (1994) and are overcome in a new set of stellar evolution calculations by increasing the OB star mass-loss rate ad hoc by a factor of two. The tracks of Meynet et al. for 40, 60, 85, and $120 M_\odot$ and $Z = 0.02$ are included in Fig. 9. They account well for the luminous hydrogen-poor WN stars (cf. Sect. 5.3). An upper luminosity limit for H-free WN stars of roughly $\log L/L_\odot = 6.0$ is predicted, which is a great advantage over the Schaller et al. tracks. However, the observed upper limit appears to be at $\log L/L_\odot \simeq 5.7$. The tracks of Meynet et al. at twice the solar metallicity, due to the even larger mass loss rates in this case, do not produce H-free WN stars above the observed limit. Therefore, the comparison with the tracks of Meynet et al. supports our conclusion that strong mass loss must occur already *during core hydrogen burning* (cf. also Maeder 1994). As the observed OB mass-loss rates are insufficient, one might speculate that the WNL-phase is actually even encountered more quickly as the consequence of rotationally induced mixing processes (cf. Fliegner & Langer 1994).

Regarding Fig. 9 it is obvious that our calculation can, in principle, account for the H-rich WNL stars, PCT-LBVs, the luminous H-poor "WNL" stars and the most luminous "WNE" stars. Note that similar conclusions as here were drawn recently by Crowther et al. (1994) on the basis of purely observational arguments. (cf. also Walborn 1989). The bulk of moderately hydrogen-rich WN stars at $\log L/L_\odot \lesssim 5.5$ appears to be related to stars of smaller initial mass. Our $60 M_\odot$ tracks shown in Fig. 1 indicate that the evolutionary scenario in the case of pulsational mass-loss rates smaller than our case $f = 1$ — which is to be expected for smaller initial masses (cf. Kiriakidis et al. 1993) — might be qualitatively different from the one discussed in the present investigation. This is also anticipated by inspection of Fig. 9, which implies that the H-rich WNL-stars are confined to large luminosities, while below $\log L/L_\odot \simeq 5.5$ the surface abundances are always smaller than $X_s \simeq 0.3$. This means that the major part of the surface enrichment from O stars to the

Wolf-Rayet phase occurs not in the hot part of the HR diagram, i.e. these objects are possibly post-red supergiant WRs.

Finally, let us mention that our evolutionary scenario might not readily apply to other galaxies, i.e. other metallicities. Not only the radiation driven mass-loss rates depend largely on the initial stellar metallicity, but also the pulsational instabilities are a sensitive function of Z (Kiriakidis et al. 1993). Consequently, the evolution of very massive stars e.g. in the Magellanic Clouds may be qualitatively different compared to the case of our Galaxy.

7. Conclusions

We have developed a novel evolutionary scenario for very massive, Galactic stars by introducing a mass-loss in addition to the radiation pressure driven wind, which is thought to be provoked by the recently discovered violent pulsational instabilities in very massive main sequence stars. We have furthermore put effort in the comparison of the resulting stellar models in the various evolutionary phases with observations, and in identifying them with corresponding observed counterparts, by the computation of stellar wind and atmosphere models, especially for the P Cygni state and for Wolf-Rayet stars. In doing so, we derived an evolutionary scenario for very massive stars, which is qualitatively different from earlier propositions in several respects.

1. Hydrogen-rich WNL-stars are identified with core hydrogen burning stars with enhanced mass-loss rates due to hydrodynamic instabilities.
2. P Cygni-type LBVs are predicted to have a very small mass for their luminosity (i.e. a large L/M-ratio) and to be strongly helium enriched, in accordance with observational evidences.
3. A second, hydrogen-poor "WNL"-phase occurs after the LBV-phase, during early core helium burning.
4. The existence of an upper luminosity limit for hydrogen-free WN stars is interpreted in terms of additional main sequence mass-loss, in support of point 1.

The proposed evolutionary sequence for very massive stars thus reads as: O → H-rich WN → PCT-LBV → H-poor WN → H-free WN → WC → SN. A variety of observational facts which are in conflict with standard evolutionary models can be qualitatively explained by this new scenario. However, also some quantitative discrepancies and open questions remain. Only further, more detailed comparisons between evolutionary tracks, calculated for different initial masses and mass-loss assumptions, with observed properties of stars will finally allow to decide which scenario is most adequate to nature.

Acknowledgements. We are grateful to P.A. Crowther, A.W. Fullerton, P. Höflich A. Maeder, and N. Walborn for helpful discussions and useful comments. Many thanks to A. Fullerton, D. Gies and T. Bolton for leaving us their unpublished material on line profile variability, and to W. Glatzel for providing the results of the pulsational analysis in electronic form. O. Stahl provided digital spectra of P Cygni. This work has been supported by the Deutsche Forschungsgemeinschaft through grants La 587/8-1, and Pa 477/1-1

References

Blaha C., Humphreys R.M., 1989, AJ 98, 1598
Bieging J.H., Abbott D.C., Churchwell E.B., 1989, ApJ 340, 518
Bressan A., Fagotto F., Bertelli G., Chiosi C., 1993, A&AS 100, 647
Crowther P.A., Willis A.J., 1994, Space Sci. Rev. 66, 85
Crowther P.A., Smith L.J., Hillier D.J., 1994, Space Sci. Rev. 66, 271
Davidson K., Moffat A.F.J., Lamers H.J.G.L.M., 1989, Physics of Luminous Blue Variables, Proc. IAU-Colloq. No. 113, Kluwer
Davidson K., Humphreys R.M., Hajian A., Terzian Y., 1994, preprint
Deacon J.R., Barlow M.J., 1991, in: IAU-Symp. 143, Wolf-Rayet Stars and interrelations with other massive stars in galaxies, K.A. Van der Hucht and B. Hidayat (eds.), Kluwer, p. 558
El Eid M.F., Hartmann D., 1993, ApJ 404, 271
Fliegner J., Langer N., 1994, in: Proc. IAU-Symp. 163, Wolf-Rayet Stars: Binaries, Colliding Winds, Evolution, ed. K. van der Hucht et al., Kluwer (in press)
Friend D.B., Poe C.H., Cassinelli J.P., 1987, BAAS 20, 1012
Fullerton A.W., 1990, Ph.D. thesis, University of Toronto
Fullerton A.W., 1991, in: Rapid variability of OB-Stars: Nature and Diagnostic Value, ed. D. Baade, ESO Workshop No. 36, p. 3
van Gent R.H., Lamers H.J.G.L.M., 1986, A&A 158, 335
Genzel R., Hollenbach D.J., Townes C.H., Eckart A., Krabbe A., Lutz D., Najarro F., 1994, in: The Nuclei of Normal Galaxies: Lessons from the Galactic Center, ed. R. Genzel, Kluwer (in press)
Glatzel W., Kiriakidis M., Fricke K.J., 1993, MNRAS 262, L7
Groenewegen M.A.T., Lamers H.J.G.L.M., 1989, A&AS 79, 359
de Groot M.J.H., Lamers H.J.G.L.M., 1992, Nat. 355, 422
Hamann W.-R., 1994, Space Sci. Rev. 66, 237
Hamann W.-R., Schwarz E., 1992, A&A 261, 523
Hamann W.-R., Dünnebeil G., Koesterke L., Schmutz W., Wessolowski U., 1991, A&A 249, 443
Hamann W.-R., Leuenhagen U., Koesterke L., Wessolowski U., 1992, A&A 255, 200
Hamann W.-R., Koesterke L., Wessolowski U., 1993, A&A 274, 397
Herrero A., Kudritzki R.P., Vilchez J.M., Kunze D., Butler K., Haser S., 1992, A&A 261, 209
Hillier D.J., 1987, ApJS 63, 947
Hillier D.J., 1989, ApJ 347, 392
Hillier D.J., 1990, A&A, 231, 116
Holzer T., 1977, J. Geophys. Res. 82, 23
Howarth I.D., Prinja R.K., 1989, ApJS 69, 527
van der Hucht K.A., Conti P.S., Lundström I., Stenholm B., 1981, Space Sci. Rev. 28, 227
Humphreys R.M., Davidson K., 1979, ApJ 232, 409
Iglesias C.A., Rogers F.J., Wilson B.G., 1992, ApJ 397, 717
Kiriakidis M., 1992, Ph.D. thesis, Universität Göttingen
Kiriakidis M., Fricke K.J., Glatzel W., 1993, MNRAS 264, 50
Koesterke L., 1993, Ph.D. thesis, Universität Kiel
Krabbe A., Genzel R., Drapatz S., Rotaciuc V., 1991, ApJ 382, L19
Kudritzki R.P., Hummer D.G., 1990, ARAA 28, 303
Kurucz R.L., 1992, Rev. Mexicana Astron. Astrof. 23, 181
Lamers H.J.G.L.M., 1986, in: Luminous Stars in Associations and Galaxies, ed. C.W.H. de Loore (Dordrecht: Reidel), p.157
Lamers H.J.G.L.M., de Groot M., Cassatella A., 1983, A&A 128,299
Lamers H.J.G.L.M., Maeder A., Schmutz W., Cassinelli J.P., 1991, ApJ 368, 538
Lamers H.J.G.L.M., Leitherer C., 1993, ApJ 412, 771

Langer N., 1989a, A&A 210, 93
Langer N., 1989b, A&A 220, 135
Langer N., 1991a, A&A 248, 531
Langer N., 1991b, A&A 252, 669
Langer N., 1992, A&A 265, L17
Langer N., 1993, in: Massive stars: their lives in the interstellar medium, ASP Conf. Ser., Vol. 35, J. Cassinelli, E.B. Churchwell, eds., p. 159
Langer N., El Eid M.F., 1986, A&A 167, 265
Langer N., Sugimoto D., Fricke K.J., 1983, A&A 126, 207
Leitherer C., 1988, ApJ 326, 356
Leitherer C., Allen R., Altner B., Damineli A., Drissen L., Idiart T., Lupie O., Nota A., Robert C., Schmutz W., Shore S., 1994, ApJ (in press)
Lucy L.B., Abbott D.C., 1993, ApJ 405, 738
Maeder A., 1983, A&A 120, 113
Maeder A., 1987, A&A 178, 159
Maeder A., 1994, in: Proc. IAU-Symp. 163, Wolf-Rayet Stars: Binaries, Colliding Winds, Evolution, ed. K. van der Hucht et al., Kluwer (in press)
Maeder A., Meynet G., 1987, A&A 182, 243
McGregor P.J., Hyland A.R., Hillier D.J., 1988a, ApJ, 324, 1071
McGregor P.J., Hillier D.J., Hyland A.R., 1988b, ApJ, 334, 639
Meynet G., Maeder A., Schaller G., Schaerer D., Charbonnel C., 1994, A&AS 103, 97
Najarro F., Hillier D.J., Kudritzki R.P., Krabbe A., Genzel R., Lutz D., Drapatz S., Geballe T.R., 1994, A&A (in press)
van den Oord G.H.J., Waters L.B.F.M., Lamers H.J.G.L.M., Abbott D.C., Bieging J.H., Churchwell E., 1985, in: Radio Stars, Astrophysics and Space Science Library, Vol.116, eds. R.M. Hjellming, D.M. Gibson, Reidel: Dordrecht, p.111
Owocki S.P., 1992, in: The Atmospheres of Early-Type Stars, eds. U. Heber and C.S. Jeffery, Springer: Berlin, p. 393
Pauldrach A.W.A., Puls J., 1990, A&A 237, 409 (Paper VIII)
Pauldrach A.W.A., Puls J., Hummer D.G., Kudritzki R.-P., 1985, A&A 148, L1
Pauldrach A., Puls J., Kudritzki R.-P., 1986, A&A 164, 86
Pauldrach A.W.A., Kudritzki R.P., Puls J., Butler K., Hunsinger J., 1994a, A&A, (in press; Paper XII)
Pauldrach A.W.A., Feldmeier A., Puls J., Kudritzki R.P., 1994b, Space. Sci. Rev. 66, 105
Puls J., 1987, A&A 184, 227
Puls J., Pauldrach A.W.A., 1991, in: Proceedings of the NATO Advanced Research Workshop on Stellar Atmospheres, "Beyond Classical Models", eds. L. Crivellari, I. Hubeny and D.G. Hummer, NATO ASI Series C, vol. 341, Kluwer: Dordrecht, p. 175
Schaller G., Schaerer D., Meynet G., Maeder A., 1992, A&AS 96, 269
Schmutz W., Hamann W.-R., Wessolowski U., 1989, A&A 210, 236
Seaton M.J., Yan Y., Mihalas D., Pradhan A.K., 1994, MNRAS (in press)
Simon K., Jonas G., Kudritzki R.P., Rahe J., 1983, A&A 125, 34
Smith L.J., Crowther P.A., Prinja R.K., 1994, A&A 281, 833
Springmann U.W.E., 1994, A&A (submitted)
Stahl O., Mandel H., Wolf B., Gäng Th., Kaufer A., Kneer R., Szeifert Th., Zhao F., 1993, A&AS 99, 167
Stothers R.B., Chin C.-W., 1981, ApJ 247, 1063
Stothers R.B., Chin C.-W., 1991, ApJ 381, L67
Stothers R.B., Chin C.-W., 1993, ApJ 408, L85
Stothers R.B., Chin C.-W., 1994, ApJ 426, L46
Vanbeveren D., 1991, A&A 252, 159
Voels S.A., Bohannan B., Abbott D.C., Hummer D.G., 1989, ApJ 340, 1073
Walborn N.R., 1989, in: Physics of Luminous Blue Variables, Proc. IAU-Colloq. No. 113, K. Davidson et al., eds., Kluwer, p. 250
Waters L.B.F.M., Wesselius P.R., 1986, A&A 155,104
Woosley S.E., Langer N., Weaver T.A., 1993, ApJ 411, 823

This article was processed by the author using Springer-Verlag LaTeX A&A style file version 3.